

# Impact of Historical Land Cover Changes on Land Surface Characteristics Over the Indian Region Using the Land Information System.

vibin jose (✉ [vibinjose20@gmail.com](mailto:vibinjose20@gmail.com))

Indian Institute of Space Science and Technology

**Anantharaman Chandrasekar**

Indian Institute of Space Science and Technology

**Suraj Reddy**

ISRO Hyderabad: National Remote Sensing Centre

---

## Research Article

**Keywords:** LSM, Noah, IMD, Land Information System (LIS)

**Posted Date:** October 19th, 2021

**DOI:** <https://doi.org/10.21203/rs.3.rs-913048/v1>

**License:**  This work is licensed under a Creative Commons Attribution 4.0 International License.

[Read Full License](#)

---

# 1 Impact of historical land cover changes on land surface characteristics 2 over the Indian region using the Land Information System

3 Vibin Jose<sup>1</sup> · Anantharaman Chandrasekar<sup>1</sup> · Suraj  
4 Reddy<sup>2</sup>

5  
6 the date of receipt and acceptance should be inserted later

7 **Abstract** The present study has employed a regional Land Surface Model (LSM) to investigate the  
8 impact of historical land cover changes on land surface characteristics over the Indian subcontinent  
9 for the period of 1930-2013. Four simulations that include a control run and three experiment runs  
10 are performed with the Noah 3.6 LSM within the Land Information System (LIS). The control run is  
11 performed with a MODIS-IGBP land cover map, while the three experimental runs are performed with  
12 three different potential land cover maps for the years 1930, 1975, and 2013. The potential land cover  
13 maps for the above three simulations are developed by blending the MODIS-IGBP data set with the  
14 fractional forest cover data set; the latter data is available for the years 1930, 1975, and 2013. Results  
15 indicate that the historical land cover change (1930 to 2013) has reduced the annual mean of latent heat  
16 flux and net surface radiation over the Indian domain by  $-24.74 W/m^2$  and  $-14.18 W/m^2$  respectively,  
17 while the sensible heat flux and the soil temperature has increased by  $4.97 W/m^2$  and 2.78 K. The  
18 annual mean change in latent heat flux, sensible heat flux, and soil temperature demonstrate that the  
19 largest changes occur when the land cover changes from forest to urban land as compared to forest to  
20 cropland, forest to grassland and forest to open shrubland. The annual mean change in latent heat flux  
21 is moderately large for the land cover change from forest to open shrubland when compared to forest  
22 to grassland and forest to cropland. The above is attributed to the effects of evapotranspiration, which  
23 has high values for the cropland followed by grassland and open shrubland. Furthermore, the triple  
24 collocation method is employed to assess the impact of historical land cover change on soil moisture.  
25 Results indicate that the triple collocation method effectively demonstrates the impact of land cover  
26 change on soil moisture.

27 **Keywords** LSM · Noah · IMD · Land Information System (LIS)

## 28 1 Introduction

29 The historical land surface changes that manifest over a country, typically occur through activities  
30 that are either (i) natural, (ii) anthropogenic or (iii) a combination of both. Deforestation refers to the

---

<sup>1</sup> Department of Earth and Space Sciences, Indian Institute of Space Science and Technology, Valiamala P.O., Thiruvananthapuram - 695 547 Kerala, India E-mail: chandra@iist.ac.in

<sup>2</sup> National Remote Sensing Centre, Indian Space Research Organization, Hyderabad, Telangana, India

31 depletion in forest areas across the world that are lost predominantly due to human activities such as (i)  
32 development of agricultural croplands, (ii) construction of urban infrastructure, and (iii) mining activities  
33 and increased urbanization. Natural forest fires, floods and diseases caused by parasites account primarily  
34 for the natural causes of deforestation. Deforestation that are caused by human activities have gained  
35 ascendancy since 1960s and their effects have accelerated in the last sixty years. Human activities are  
36 considered to be primarily responsible for deforestation globally with expansion of agricultural activity  
37 accounting for nearly 80% of the global forest cover loss. Construction of urban infrastructure (15%)  
38 and mining activities together with increased urbanization (5%) are the other human factors that are  
39 responsible for loss of forest cover worldwide. Deforestation not only impacts the atmospheric circulation  
40 (Dong et al., 2019; Deng et al., 2013; Dirmeyer et al., 2010) but also affects natural ecosystem, biodiversity  
41 and climate. Land cover changes are known to impact the climate through changes in surface albedo,  
42 sensible and latent heat fluxes, soil moisture, and soil temperature (Pitman, 2003; Pielke et al., 1998).  
43 Anyanwu (2015) and Tyagi et al. (2013) in their studies found that dense forest have higher soil moisture  
44 (SM) content as compared to degraded forest due to higher infiltration, dense roots, and higher organic  
45 content under dense forest. Earlier studies that have investigated the impact of deforestation have shown  
46 that strong cooling over the mid-latitude region is obtained (Betts, 2001; Betts et al., 2007; Hansen  
47 et al., 2005; Kvalevåg et al., 2010; Cherubini et al., 2018). The above result suggests that changes  
48 in albedo are a more dominant factor as compared to changes in evapotranspiration in determining  
49 the impact of deforestation over the mid-latitude regions (Betts, 2001; Hansen et al., 2005; Huang  
50 et al., 2020). However, over tropical regions, various studies have conclusively shown that the effects of  
51 evapotranspiration play a more dominant and important role as compared to changes in albedo, leading  
52 to surface warming over tropics (Bounoua et al., 2002; Bonan, 2008; Garratt, 1993; Feddema et al., 2005;  
53 Sampaio et al., 2007; Davin and de NOBLET, 2010; Lawrence and Chase, 2010; Pitman et al., 2012;  
54 Findell et al., 2006). Land cover changes are known to alter the characteristics of the land surface such as  
55 roughness length, leaf area index, stem area index, and surface albedo (Liu et al., 2015; Guo et al., 2016;  
56 Nair et al., 2011). Kvalevåg et al. (2010), show that impacts of deforestation leads to a reduction of (i)  
57 the rooting depth, (ii) stem area index, (iii) leaf area index, and (iv) roughness length, respectively. The  
58 reduction in the values of leaf area index, surface roughness, and vegetation cover contribute to lower  
59 rates of evapotranspiration (Pitman, 2003; Liu et al., 2019; Peng et al., 2014; Bright et al., 2017).

60 It is generally a well-accepted fact that as the surface albedo increases (with decreased forest cover),  
61 more solar radiation is reflected by the surface and the net effect will be surface cooling. Also, it is  
62 known that the reduced roughness length (with decreased forests) can contribute to reduced latent and  
63 sensible heat fluxes that results in surface warming (Liu et al., 2014). Furthermore the deep rooted forest  
64 vegetation that can access deep soil layers results in an increase in transpiration and latent heat flux  
65 and hence consequently to a decrease in sensible heat flux (from surface energy budget), as compared to  
66 a crop land or pasture region (Pielke et al., 2011).

67 Observational records indicate that there have been extensive changes in land cover over the past  
68 hundred years over the Indian region, which has directly or indirectly affected the resultant climate. The  
69 percentage of deforested area over the Indian region in the last nine decades (1930-2013) is estimated  
70 as 28.01% (Reddy et al., 2018). There are several studies addressing the impact of land use/land cover  
71 change on the Indian summer monsoon region (Niyogi et al., 2018, 2010; Dutta et al., 2009; Halder et al.,

2016). Gogoi et al. (2019) investigated the effect of land use/land cover (LULC) change on the surface air temperature over the eastern state (Odisha) of India using observations and reanalysis products. The results of the aforementioned study indicate that the mean surface air temperature over the state of Odisha has increased by  $0.3^{\circ}\text{C}$  during the period 1981 to 2010 and about 25 to 50 % of surface air warming is closely related to land use/land cover change. Halder et al. (2016) studied the impact of LULC change on the surface air temperature over the Indian domain using high-resolution regional climate model during 1951 through 2005. Results show a warming effect on daily mean and extreme temperature by  $1\text{-}1.2^{\circ}\text{C}$  over central India. However, over India, most of the aforementioned studies have focused on the impacts of LULC on India summer monsoon rainfall and surface air temperature; with very little emphasis on the impact of LULC changes on the surface energy fluxes, soil moisture and soil temperature, respectively. In order to address the above objective, the present study, investigates the impact of historical land cover changes over the Indian region for a 83 year period on the land surface characteristics such as (i) surface energy fluxes (latent and sensible heat flux), (ii) soil temperature (ST), and (iii) soil moisture using the Noah land surface model (LSM).

In the following section, descriptions of the Model, data, and methodology are provided. While Section 3, describes the Experimental design. the Results and discussion are provided in section 4, Section 5 brings out the broad conclusions of the study.

## 2 Model, data, and methodology

### 2.1 LIS (Land Information System) and LSM

LIS is a software framework developed by NASA Goddard Space Flight Center for land surface modeling and data assimilation (Kumar et al., 2006). This software includes several land surface models that can be run on global or regional domains with horizontal resolution as high as 1 km. LIS integrates parallel high performance computing and communications technologies with modern land surface modeling techniques and data assimilation routines.

The present study uses the LIS software framework for running the Noah 3.6 land surface model (LSM) in offline mode (not coupled with atmospheric models) over the Indian subcontinent, that extends from  $6.375^{\circ}\text{N}$  to  $38.375^{\circ}\text{N}$  and  $66.375^{\circ}\text{E}$  to  $99.875^{\circ}\text{E}$  with a spatial resolution of 4 km. The development of Noah LSM (Chen et al., 1996) is initiated by the four agencies, National Center for Atmospheric Research, Oregon State University, U.S. Air Force, and National Centers for Environmental Prediction's Office of Hydrology. The Noah LSM may be used either as uncoupled mode or embedded within an atmospheric model. The Noah LSM calculates soil moisture and soil temperature over four soil depths (0-0.1 m, 0.10-0.30 m, 0.30-0.60 m, 0.60-1 m). The Noah LSM requires the following inputs to simulate the land surface processes over time, (i) land surface parameters, which include land cover data, soil texture, surface albedo, and greenness fraction etc, (ii) atmospheric forcings that include surface meteorology, surface radiation components and precipitation, and (iii) initial land surface state.

## 2.2 Land surface parameter data sets

The present study uses the Moderate Resolution Imaging Spectroradiometer-International Geosphere-Biosphere Programme (MODIS-IGBP) land cover data and temporal fractional forest cover data over the Indian region. The MODIS-IGBP data has twenty land cover classes at a spatial resolution of 0.9 km (30 s) (Friedl et al., 2002). The fractional forest cover data is developed using multi-source and multi-temporal remote sensing data for the years 1930, 1975 and 2013 by Reddy et al. (2018) and is made available through NICES portal of National Remote Sensing Centre, Indian Space Research Organization (<https://bhuvan-app3.nrsc.gov.in/data/download/index.php?c=p&s=NI&g=OS>). The fractional forest cover information was primarily based on classification of forest cover and subsequent spatial grid-analysis at 5km scales. For this study, we have used an identical grid surface as of MODIS-IGBP land cover data so as to overlay and generate potential land-cover maps (for more details refer Section 2.2.1). The forest cover for the year 1930 is generated using the topographical maps (1:250,000 scale) prepared by US ARMY services during the years 1920 - 1940. The 1975 forest cover information is obtained using Landsat Multi-spectral Scanner (MSS) data from 1972-1977 over Indian region. Indian Remote Sensing (IRS) satellite Resourcesat-2 AWiFS data was used to generate 2013 forest mask. All the remote sensing data sets are subjected to noise removal and precise geometric corrections before classification of forest cover. The atmospheric corrections were also performed using the top-of-atmosphere reflectance algorithms. The interpretation of remote-sensing data sets was carried out using a hybrid approach of digital image classification and visual interpretation to minimize the changes associated with sensor differences as well as with phenological, atmospheric and environmental variability. Multi-source data sets corresponding to 1920-1940, 1972-1977, and 2013-2014 are being referred to as 1930, 1975, and 2013 periods respectively. The soil texture map data has been taken from State Soil Geographic-Food and Agriculture Organization (STATSGO-FAO) soil texture map. It has 16 soil texture classes with a spatial resolution of 0.9 km (30 s). The elevation data is provided by the Shuttle Radar Topography Mission (SRTM) data. The greenness fraction, slope type, and albedo data sets are taken from National Centers for Environmental Prediction (NCEP) data sets. International Satellite Land Surface Climatology Project 1 (ISLSCP1) bottom temperature data sets are utilized for the bottom temperature data for the present study. Figure 1 shows the regions where the historical land cover changes with significant depletion in forest cover have manifested over the Indian domain between the years 1930 and 2013. It is clear from Figure 1 that significant depletion in forest cover over the Indian domain between the years 1930 and 2013 is restricted to regions that represent some areas of (i) North India, (ii) Central India, (iii) Northeast India, and (iv) Western ghats.

### 2.2.1 Preparation of potential land cover map

Since the fractional forest cover information is void of any classification information on other land-use land cover classes, we have generated potential land cover maps by blending MODIS-IGBP land cover information with the temporal fractional forest cover data. The land cover types are fixed to a single land cover class for each grid point in the Noah model, while the preparation of potential land cover is performed by using an appropriate cutoff value of 0.5. If the fraction of forest cover in a grid point is above the cutoff value of 0.5, the corresponding grid point in the potential land cover map is represented

146 by a single land cover type. The cutoff value was appropriately chosen in such a way that it satisfied the  
147 following requirement; number of grid points that manifested change between 1930 potential land cover  
148 and 2013 potential land cover are reflect the actual change between the 1930 and 2013 fractional forest  
149 cover data. The preparation of potential land cover map is performed in the following two steps. In the  
150 first step, the potential land cover map of year 2013 is generated by modifying the MODIS-IGBP non-  
151 forest vegetation (such as croplands, urban and built-up, cropland mosaics, bare soil and rocks) to forest  
152 vegetation class, if the corresponding grid point in the fractional forest cover data has value above 0.5.  
153 Also, the forest cover class information for such grids with only fractional forest cover data is fashioned  
154 on the assumption that it would be similar to the adjacent forest vegetation class. Applying the aforesaid  
155 idea, each forest vegetation grid point in the MODIS-IGBP land cover map is replaced by nearby non-  
156 forest vegetation, provided the corresponding grid point in the fractional forest cover data has a value  
157 below 0.5. In the second step, the potential land-cover map of 2013 is used in the generation of potential  
158 land cover map for 1975 by replacing the non-forest vegetation of each grid point in the 2013 layer to  
159 nearby forest vegetation by checking the corresponding grid in the 1975 fractional forest cover data and  
160 ascertaining that the fractional forest cover data has a value above 0.5 at that grid point. Additionally,  
161 the potential cover data for the year 1930 (refer Figure 2) is prepared by changing 1975 potential cover  
162 data using the 1930 fraction forest cover data by following the aforementioned methodology.

### 163 *2.2.2 Modified soil texture, albedo, and greenness fraction data sets*

164 The land surface parameters such as soil texture, albedo, greenness fraction are also suitably modified  
165 every time the potential land cover map is generated. The present study has obtained the soil texture data  
166 from the State Soil Geographic-Food and Agriculture Organization (STATSGO-FAO) soil texture map.  
167 The soil texture at a grid point corresponding to the modified vegetation is replaced by the dominant  
168 soil texture that corresponds to the appropriate modified vegetation class of MODIS-IGBP data over  
169 the Indian domain. For example, assume that a grid point corresponding to the modified vegetation is  
170 Evergreen broad leaf forest as land cover. Then the corresponding dominant soil texture for the Evergreen  
171 broad leaf forest class over the Indian domain is identified and let it be “clay loam”. The soil texture  
172 at the identified grid point over which the landcover is being changed is then modified to “clay loam”  
173 type. The albedo and Greenness fraction data sets are obtained from NCEP data sets with a spatial  
174 resolution of  $0.01^\circ \times 0.01^\circ$ . The greenness fraction and albedo values for the altered vegetation grids are  
175 replaced every month by taking the mid-value of the above land surface parameters over the range of  
176 values corresponding to each vegetation class that is observed over the Indian domain.

### 177 *2.3 Meteorological forcing data*

178 The meteorological forcing data are obtained from Global Data Assimilation System (GDAS) and Indian  
179 Meteorological Department (IMD) rainfall data. The NCEP GDAS Final (FNL) operational global  
180 analysis data (Rodell et al., 2004) is available with a spatial resolution of  $0.25^\circ \times 0.25^\circ$  and operationally  
181 at every six hours. The GDAS data has assimilated surface observations, aircraft reports, balloon data,  
182 radar observations, wind profiler data, and satellite observations into a gridded model space by employing  
183 a four-dimensional multivariate method.

184 The Indian Meteorological Department (IMD) gridded rainfall data is prepared using daily rainfall  
185 records from a dense network of 6955 rain gauge stations over the Indian region (Pai et al., 2014).  
186 The high spatial resolution IMD gridded data set is developed by using an inverse distance weighted  
187 interpolation (IDW) scheme. The above data set is available as 24 hr accumulated rainfall data with a  
188 high spatial resolution of  $0.25^\circ \times 0.25^\circ$

## 189 2.4 Triple collocation (TC) method

190 The present study has evaluated the impact of land cover change on soil moisture estimate using triple  
191 collocation (TC) method. While the above method was proposed initially by Stoffelen (1998) for ocean  
192 studies, in subsequent years the TC method has been widely employed in soil moisture studies (Wu  
193 et al., 2020; Kolassa et al., 2017; Nair and Indu, 2019). The basic idea of TC method relies on the  
194 availability of three independent measurements of the same variable. The error covariance of these data  
195 sets are obtained by data collocation (Gruber et al., 2017; Wu et al., 2020). For the present study, TC  
196 based Extended Triple Collocation (ETC) method is adopted from McColl et al. (2014). To ensure that  
197 the assumptions of the TC method are applicable, the present study has utilized soil moisture estimates  
198 from MERRA (Modern-Era Retrospective analysis for Research and Applications) Land data and Global  
199 Land Data Assimilation System (GLDAS) Catchment Land Surface Model (CLSM), data set along with  
200 the 1930 potential land cover simulation as the triad of independent measurements on soil moisture.  
201 Furthermore, soil moisture data from MERRA, GLDAS and the 2013 potential land cover simulation  
202 constitute a second triad of independent measurements of soil moisture.

## 203 2.5 Model initialization

### 204 2.5.1 LIS spin up

205 Obtaining accurate land surface initialization in a LSM is critical for deriving the evolution of the land  
206 surface characteristics with time (Dirmeyer and Halder, 2016). Initial conditions for land surface models  
207 are obtained through spin up process (Rodell et al., 2005). The present study employed a common  
208 method for initializing the Noah LSM, by spinning up the LSM through several iterations repeatedly  
209 through a single year until the soil equilibrium is reached.

210 In this study, all the four simulations were initialized by running the Noah LSM forced with the same  
211 land and atmospheric parameters except that the land cover map, albedo, soil texture, and greenness  
212 fraction data are different for the four simulations. Table.1 lists the summary of model and data utilized  
213 in this study. For obtaining the initial condition on 01 June 2013 00 UTC, the Noah LSM is integrated  
214 by assuming an initial soil moisture and soil temperature values as  $0.15 \text{ m}^3/\text{m}^3$  and 298 K at all four  
215 layers and all grid cells on 01 June 2012 00 UTC. The Noah LSM is then integrated for an year till 01  
216 June 2013 00 UTC (first loop). The Noah LSM is then integrated again for the above same period (2nd  
217 loop) by reassigning the initial values of land surface variables on 01 June 2012 00 UTC with 01 June  
218 2013 00 UTC. The above step is repeated until the changes in the deepest layer (0.60-1 m) soil moisture  
219 differences between the successive loops is less than 5%.

### 220 3 Experimental design

221 The impact of historical land cover change on land surface characteristics over the Indian region is  
 222 investigated using the Noah LSM with historical fractional forest cover maps over the Indian region.  
 223 The present study conducted the control run and three experimental runs. In the control run (Ctl-run),  
 224 the Noah LSM is forced with meteorological forcing data from GDAS and IMD (rainfall data) data  
 225 and the land surface parameters such as land cover, soil texture, albedo, and greenness fraction are  
 226 obtained from MODIS-IGBP land cover map, STATSGO-FAO soil texture map, and NCEP (albedo  
 227 and greenness fraction) data sets respectively. The remaining three experimental runs are conducted by  
 228 forcing the Noah LSM with the same land and atmospheric parameters as that of the Ctl-run, except  
 229 that the land cover map, albedo, soil texture, and greenness fraction data are different for the three  
 230 simulations. For the three experimental runs, the land cover data sets are derived from MODIS-IGBP  
 231 data using fractional forest cover maps of 2013, 1975 and 1930, respectively. The soil texture, albedo,  
 232 and greenness fraction are also modified from the corresponding data sets (STATSGO-FAO, NCEP) for  
 233 the three experimental runs. The experimental run, which uses the potential land cover map for 1930,  
 234 1975, and 2013 is hereafter identified as Exp1-run, Exp2-run, and Exp3-run respectively. The model  
 235 runs, and the type of input data sets used in the model are given in Table 2.

236 All the four model LSM simulations are initiated from 01 June 2013 00 UTC and integrated for  
 237 a period of one year over the Indian region that extends from 6.375°N to 38.375°N and 66.375°E to  
 238 99.875°E with 4km horizontal spatial resolution.

**Table 1** Model and data used

Model used	Model resolution	Land parameters used	Meteorological forcing used (GDAS)	Precipitation data (resolution)
Noah 3.6	4 km	Potential land cover	Near surface air temperature	IMD (0.25°×0.25°)
		Modified soil texture	Near surface specific Humidity (kg/kg)	
		SRTM(Elevation)	Incident shortwave radiation ( $\frac{W}{m^2}$ )	
		Modified monthly albedo	Incident longwave radiation ( $\frac{W}{m^2}$ )	
		NCEP(Maximum snow albedo)	Near surface zonal wind ( $\frac{m}{s}$ )	
		NCEP(slope type)	Near surface meridional wind ( $\frac{m}{s}$ )	
		Modified Greenness fraction	Surface pressure (Pa)	
		ISLSCP1(Bottom temperature)	Convective rainfall rate ( $\frac{kg}{m^2}$ )	

### 239 4 Results and Discussions

#### 240 4.1 Impacts on land surface characteristics

241 The potential impact of land cover change on surface variables is substantial only over regions where  
 242 the direct land cover changes are observed (Chase, 1999). For the present study, regions of direct land  
 243 cover changes are selected (Western ghats, Central India, North India, and Northeast India) to analyze  
 244 the impact of land cover changes on land surface characteristics (refer Figure 1). Since the change in the  
 245 fractional forest cover map for the years 2013 and 1975 are not significantly different from one another  
 246 (refer Figure 2), the land surface characteristics are similar for the Exp2-run and Exp3-run over India for  
 247 all seasons. Although Figure 3 and Figures 6 to 9 depict the model output from all three experimental

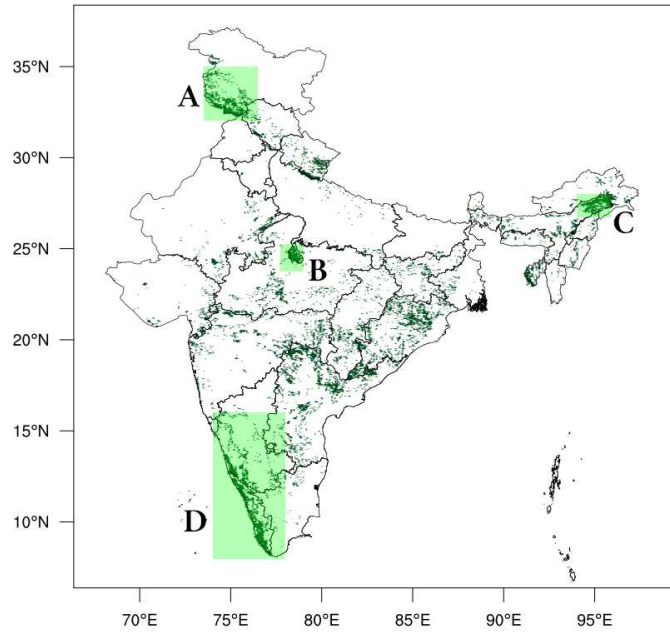


**Fig. 1** The significant change in forest cover between the years 1930 and 2013 over the Indian domain. The rectangular shaded regions represent North India (A), Central India (B), Northeast India (C), and Western ghats (D), where the land cover changes are significant.

248 runs, considering the closeness of the results of Exp2-run and Exp3-run, the discussion of the results  
 249 would be confined mostly to the simulation of Exp1-run and Exp3-run, respectively.

#### 250 4.1.1 Impacts on soil moisture and soil temperature

251 Land use/land cover plays a crucial role in regulating the spatial and temporal variation of soil moisture  
 252 (SM) by influencing the following processes such as runoff, infiltration, and evapotranspiration (Niu  
 253 et al., 2015). Figure 3 shows the time series of daily mean SM spatially averaged over Central India,  
 254 North India, Northeast India, and Western ghats at 5 cm depth for different seasons and for all the  
 255 three experiment run simulations. The spatial averaged SM over a particular region, say, Central India  
 256 would average the SM over all the grid points that encompass that region, i.e., over Central India. All  
 257 regions show high SM values during the monsoon season. This is attributed to the fact that India, as a  
 258 whole, receives 85 % of annual rainfall during the monsoon season. From figure 3, it is clear that the SM  
 259 estimates from the Exp1-run show a noticeably higher value than that of Exp3-run for all regions and  
 260 all seasons, except for the North Indian region, where the Exp1-run SM values are lower as compared  
 261 to the other two simulations. The explanation for the above is that the modified soil texture for Exp1-  
 262 run over the North Indian region has low field capacity and lower porosity values as compared to the  
 263 Exp3-run. From Figure 4, it is evident that over the North Indian region, the soil texture classified as  
 264 Clay (Porosity value (0.455) and Field capacity value (0.38)) and Clay loam (Porosity value (0.448)  
 265 and Field capacity value (0.362)) for the Exp3-run are changed to Loamy soil texture (Porosity value  
 266 (0.438) and Field capacity value (0.335)) for the Exp1-run. The Clay and Clay loam soils have a higher  
 267 field capacity, higher porosity, and lower soil conductivity values as compared to Loamy soil; thus, soil  
 268 water drains more rapidly in the Loamy soil layers as sub-surface runoff, which reduces the SM over the

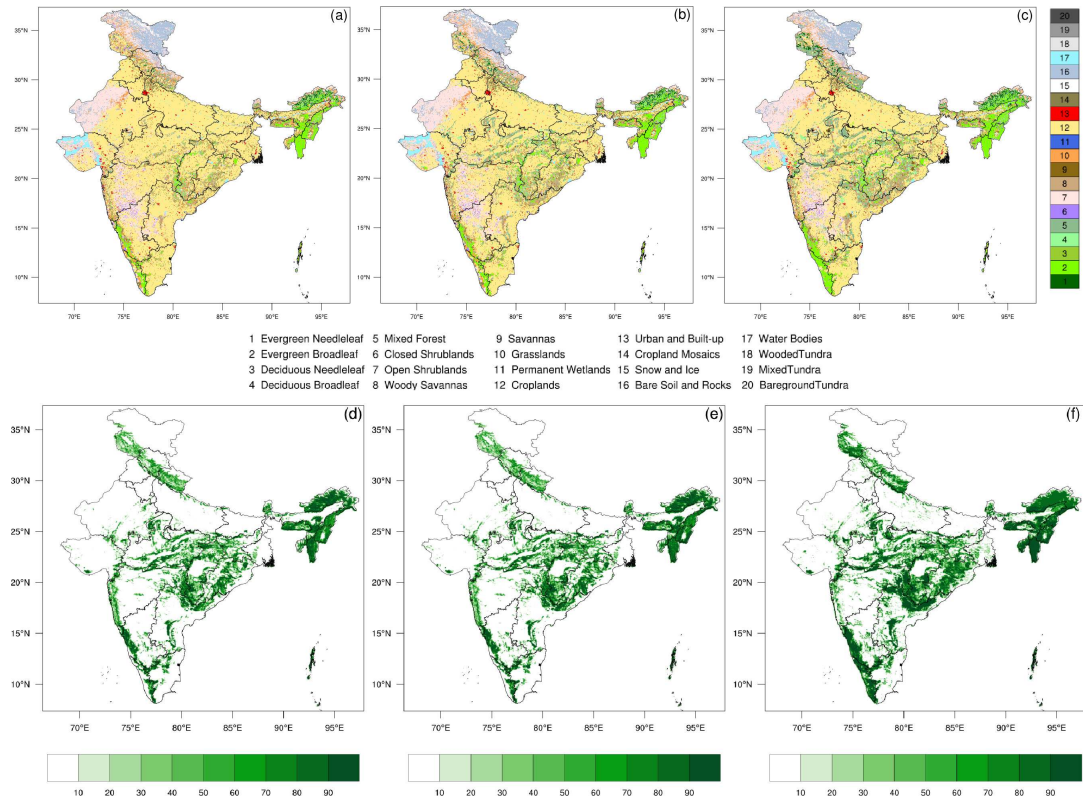


**Fig. 2** The potential land cover map (a), (b), and (c) (top panel) and the fractional forest cover map (percentage) (d), (e), and (f) (bottom panel) for the years 2013, 1975, and 1930 respectively.

269 North Indian region. The above feature is observed for North Indian region over all the four seasons.  
 270 Over the Western Ghats, for Exp1-run, the modified soil texture is classified as Clay Loam (refer to  
 271 Figure 4); while in Exp3-run, the modified soil texture is classified as Loam. The SM estimates in the  
 272 Exp1-run are higher than the Exp3-run over the Western ghats for all the four seasons. The Loam soil  
 273 texture is associated with coarser particles as compared to Clay Loam. It is well known that the soil  
 274 conductivity increases with the increase of coarser particle size. Soil electrical conductivity is a measure  
 275 of the amount of salts in the soil. It is known that soils having excess salt content hinders plant growth  
 276 and hence such soil with high soil conductivity are associated with arid and semi-arid environments  
 277 that have lower SM values. The aforementioned argument explains the increase in SM for the Exp1-run  
 278 over the Western ghats as compared to Exp3-run for all the four seasons. Similarly, over Central India  
 279 and Northeast India, Exp1-run has higher SM as compared to Exp3-run for all the four seasons. The  
 280 change in SM estimates between Exp1-run and Exp3-run is higher over Central India and Northeast  
 281 India as compared to Western ghats for all the four seasons. The aforesaid observation is attributed to  
 282 the fact that the change in spatially averaged porosity values is also higher over those regions. During the  
 283 monsoon season, the SM differences between the Exp3-run and Exp1-run are quite low for all regions.  
 284 This is because precipitation is the most critical parameter for land surface modeling compared to the  
 285 other land and atmospheric forcing parameters. From Figure 3, it is clear that during dry seasons the soil  
 286 moisture estimates are higher for the Exp1-run as compared to Exp3-run, except for the North Indian  
 287 region.

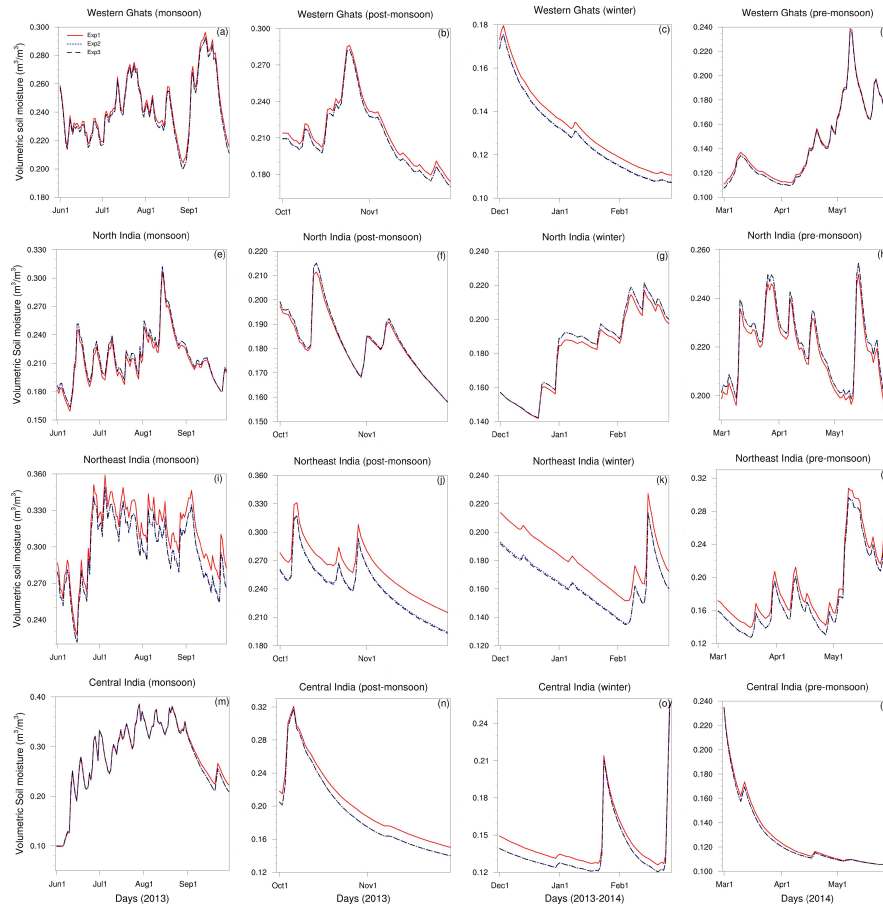


**Fig. 3** Time series of daily mean soil moisture spatially averaged over Central India, North India, Northeast India, and Western Ghats at 5 cm depth for different seasons for all three experimental runs.

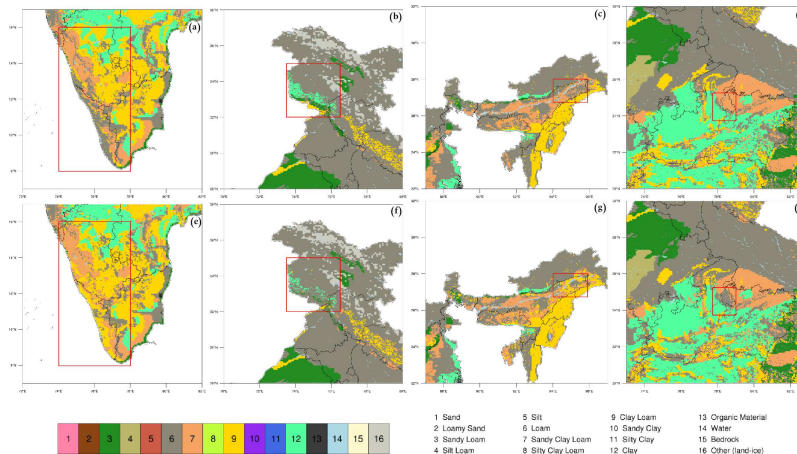


**Fig. 4** Modified soil texture map derived from STATSGO-FAO soil texture map for the years 2013 (top panel) and 1930 (bottom panel) over Western Ghats (a), North India (b), Northeast India (c), and Central India (d).

288 Furthermore, the impact of land cover change on SM is evaluated using triple collocation (TC)  
 289 method. Two groups of triplets are employed for the TC analysis. The SM obtained from GLDAS  
 290 CLSM and MERRA Land data are both utilized as two independent measurements kept same for both  
 291 triplets while the third independent measurement is the SM in each of the two triplet group, i.e., SM  
 292 from Exp1 and Exp3 SM simulations. The TC analysis is performed for the entire study period and the

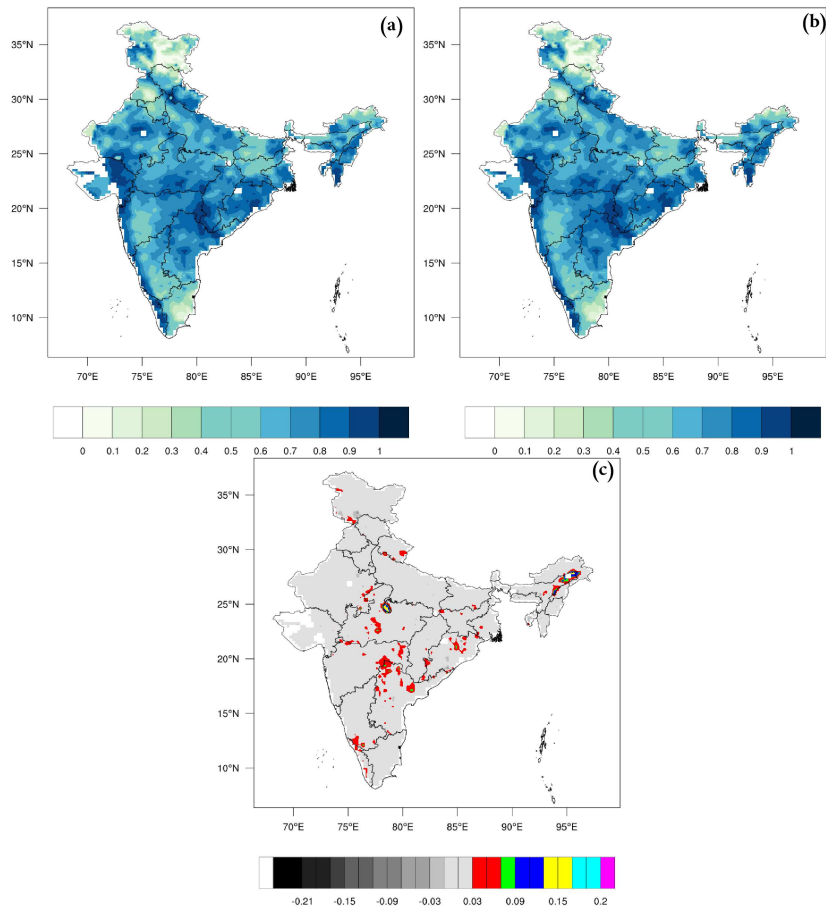


**Fig. 5** Squared correlation coefficient obtained using TC method for (a) Exp1 run and (b) Exp3 run soil moisture, (c) depicts the change in squared correlation coefficient of Exp1 and Exp3.

293 squared correlation coefficients are obtained by adopting McColl et al. (2014) approach. Figures 5a and  
 294 5b show the squared correlation coefficient of Exp1 and Exp3 SM estimate, while Figure 5c depicts the  
 295 change in squared correlation coefficient of Exp1 and Exp3 SM estimate. From Figures 5c it is clear that  
 296 the change in squared correlation coefficient is having higher values over those regions where the land  
 297 cover changes are significant (refer to Figure 1). The above results indicate that the TC analysis has  
 298 effectively captured the impact of land cover change on SM.

299 The daily cycle of soil temperature primarily depends on the position of the sun and air temperature.  
 300 However, factors such as land cover and soil moisture also play an important role in the daily soil  
 301 temperature (ST) cycle. It is known that the high SM content and the effect of land cover shading will  
 302 result in a decrease in the soil temperature. Additionally, the low SM values will contribute to increased  
 303 soil temperature values; the aforementioned effect will however be weaker below forest canopies than  
 304 grasslands (Lozano-Parra et al., 2018). Figure 6 shows the time series of daily mean soil temperature  
 305 spatially averaged over Central India, North India, Northeast India, and Western ghats at 5 cm depth  
 306 for different seasons and for all the three experimental runs. From Figure 6, it is clear that the soil  
 307 temperature (ST) attains its lowest value during the winter season and its highest value during the  
 308 end of the pre-monsoon season. The aforementioned observation can be explained due to the low solar  
 309 radiation during winter season while the highest ST value is attained during the season that has dominant  
 310 solar radiation accompanied by very limited cloud cover. The results of Exp1-run shows a decrease in

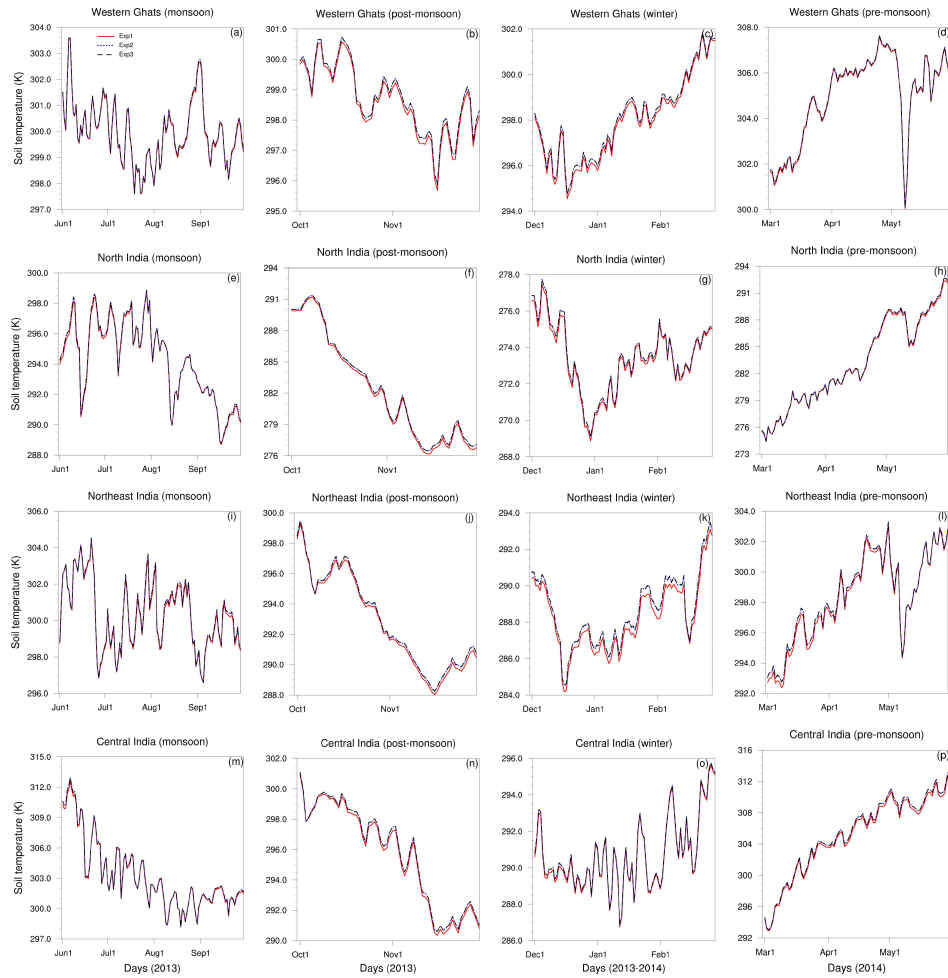


**Fig. 6** Time series of daily mean soil temperature spatially averaged over Central India, North India, Northeast India, and Western ghats at 5 cm depth for different seasons for all three experimental runs.

311 soil temperature as compared to Exp3-run for all regions and all seasons (refer Figure 6). It is known  
 312 that the removal of trees (reduced forest cover in Exp3-run) decreases the shading of the surface which  
 313 will have a warming effect on the land surface contributing to a slight increase in the soil temperature  
 314 in Exp3-run. Additionally, the decrease in evaporation rate for the Exp3-run due to low soil moisture  
 315 values (refer Figure 3) provides additional available energy at the surface leading to an increase in soil  
 316 temperature values.

#### 317 4.2 Impacts on surface fluxes

318 Figures 7 and 8 show the time series of daily mean latent heat and sensible heat flux (LHF and SHF)  
 319 spatially averaged over Central India, North India, Northeast India, and Western ghats for different  
 320 seasons and for all the three experimental run simulations. The LHF during winter season is lower for  
 321 all four regions as compared to the other three seasons for all experimental simulations, indicating lower  
 322 evapotranspiration due to reduced soil moisture during the winter season. For all four regions, the Exp1-  
 323 run shows increased LHF values as compared to the Exp3-run for all the seasons. This is due to the  
 324 increased SM availability in Exp1-run as compared to Exp3-run. Additionally, the increased transpiration

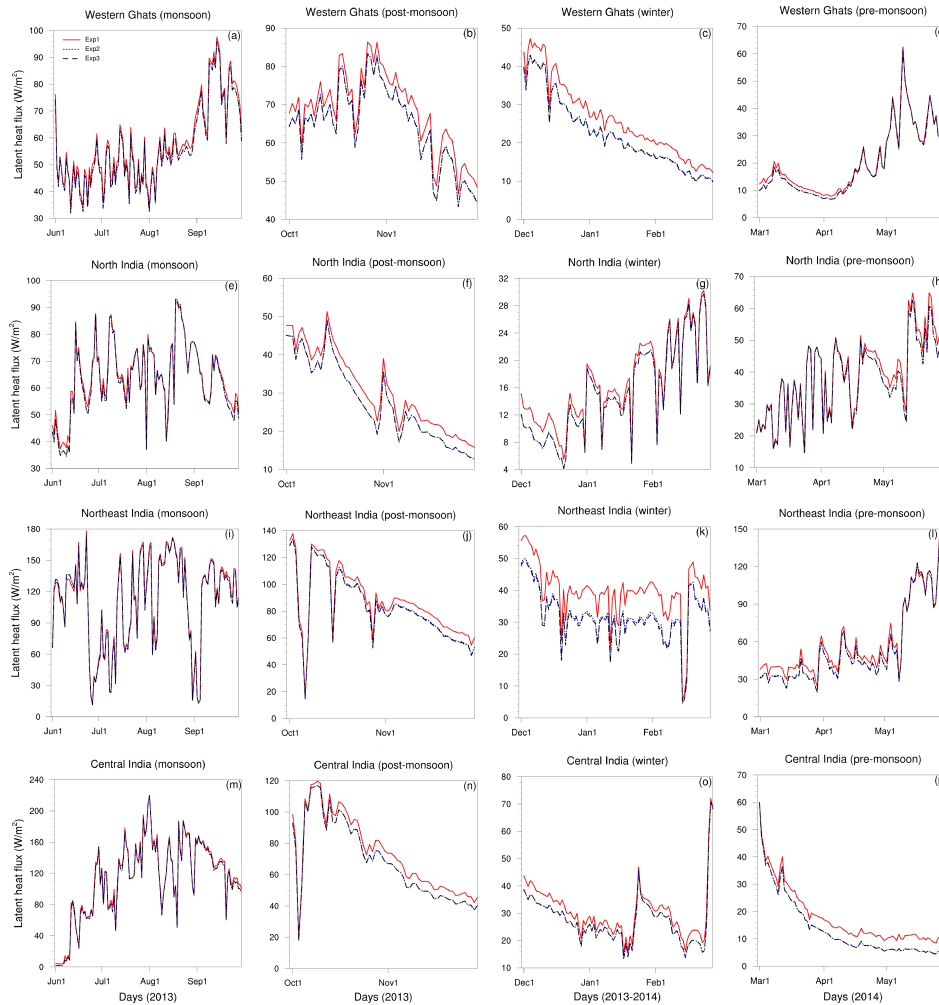


**Fig. 7** Time series of daily mean latent heat flux spatially averaged over Central India, North India, Northeast India, and Western ghats for different seasons for all three experimental runs.

325 and canopy evaporation in the Exp1-run resulting from increased greenness fraction and the changes in  
 326 land cover also contributes to an increase in LHF value for the Exp1-run. Furthermore, the conversion of  
 327 cropland to forest land results in an increase of higher surface roughness, which increases the turbulent  
 328 driven latent heat flux between the land surface and the atmosphere (Lee and Berbery, 2012). The  
 329 change of LHF value between Exp1-run and Exp3-run in the seasonal mean of LHF is maximum for  
 330 the post-monsoon season and winter season for all regions, while the minimum value of the difference of  
 331 mean LHF between the Exp1-run and Exp3-run is attained in the monsoon season. The aforementioned  
 332 observation can be explained by advancing the following argument. It is clear from Figure 3 that the  
 333 difference of SM value between Exp1-run and Exp3-run are lowest during the monsoon season over all  
 334 the four regions. Furthermore, the difference of SM value between Exp1-run and Exp3-run are highest  
 335 during the post-monsoon season and winter season (refer Figure 3). It is clear that the latent heat flux  
 336 will most definitely reflect the signature of the soil moisture.

337 Figure 8 shows a consistent annual mean reduction in SHF for Exp1-run as compared to Exp3-run  
 338 for all the regions and all the seasons. The reason for the above, is that for Exp3-run, the shrubs and  
 339 grasses lands are incapable of liberating the same flux of moisture in the Exp3-run in the form of LHF

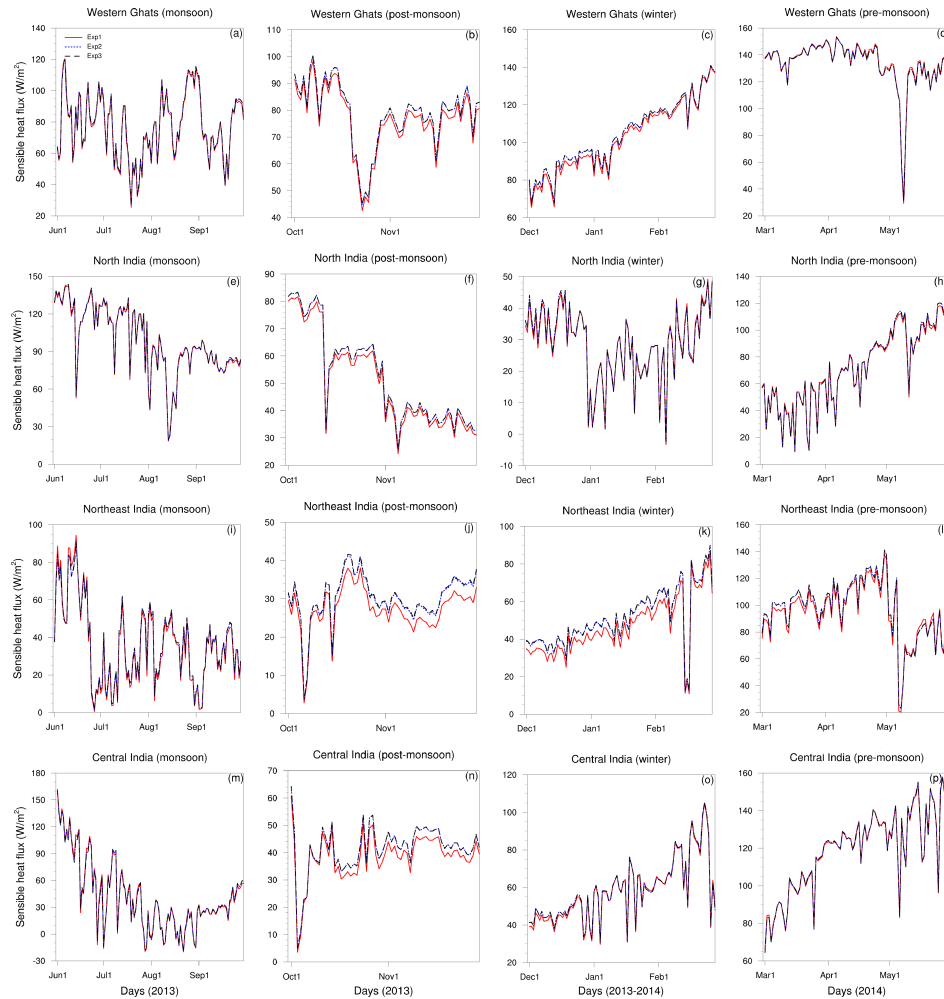


**Fig. 8** Time series of daily mean sensible heat flux spatially averaged over Central India, North India, Northeast India, and Western ghats for different seasons for all three experimental runs.

340 as the forest cover. Due to the above reason, evaporative cooling decreases with an increase in the  
 341 soil temperature, and SHF for the Exp3-run. In addition, the shallow-rooted vegetation, that cannot  
 342 access water from deeper soil layers will experience a decrease in transpiration in Exp3-run and hence  
 343 consequently an increase in SHF value for Exp3-run as compared to deep-rooted vegetation.

344 Figure 9 shows the time series of daily mean net surface radiation (NSR) spatially averaged over  
 345 Central India, North India, Northeast India, and Western ghats for different seasons and for all the three  
 346 experimental runs. Similar to the LHF and SHF, the NSR also shows lower values during the winter  
 347 season as compared to the other three seasons and for all the four regions. The results of Figure 9 shows  
 348 that the NSR value shows an increase in Exp1-run as compared to Exp3-run. NSR typically depends on  
 349 land surface albedo, and outgoing longwave radiation. Figure 10 depicts the time series of monthly mean  
 350 albedo and greenness fraction for Exp1-run and Exp3-run, that is spatially averaged over Western ghats  
 351 (a), North India (b), Northeast India (c), and Central India (d). The spatial averaging in Figure 10 of  
 352 the albedo and the greenness fraction over a region is averaged over all the grid points that encompass  
 353 that region. It is clear from Figure 10 that the mean albedo and mean greenness fraction of Exp1-  
 354 run is consistently higher as compared to the Exp3-run. The aforementioned observation is consistent  
 355 with the present understanding of the land-atmosphere interaction processes. It is clear from Figure 10

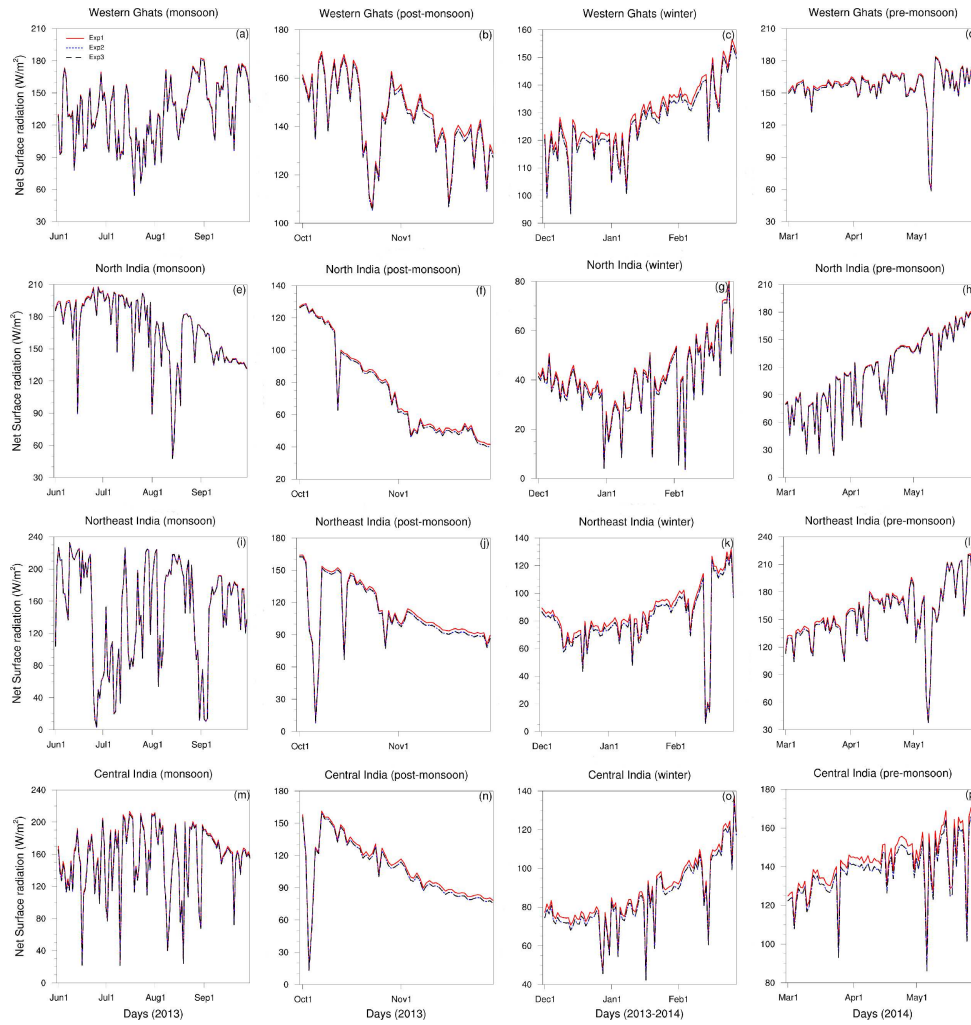


**Fig. 9** Time series of daily mean Net Surface radiation spatially averaged over Central India, North India, Northeast India, and Western ghats for different seasons for all three experimental runs.

**Table 2** Summary of simulations

Simulation	Land cover	Soil texture		Albedo and Greenness fraction
Ctl-run	MODIS-IGBP	STATSGO-FAO		NCEP
Exp1-run	Potential land cover (1930)	Modified (1930)	STATSGO-FAO	modified NCEP (1930)
Exp2-run	Potential land cover (1975)	Modified (1975)	STATSGO-FAO	modified NCEP (1975)
Exp3-run	Potential land cover (2013)	Modified (2013)	STATSGO-FAO	modified NCEP (2013)

356 that Exp3-run corresponds to higher albedo and higher outgoing long wave radiation (due to higher  
 357 soil temperature) and hence it is clear that Exp3-run has consistently higher NSR values as compared  
 358 to Exp1-run. It is clear from Figure 10 that for all the four regions, the albedo is maximum for both  
 359 Exp1-run and Exp3-run during the July-August months. Both July and August months correspond to  
 360 southwest Indian monsoon season which is characterized by extreme cloudiness and heavy rainfall over  
 361 most of India.

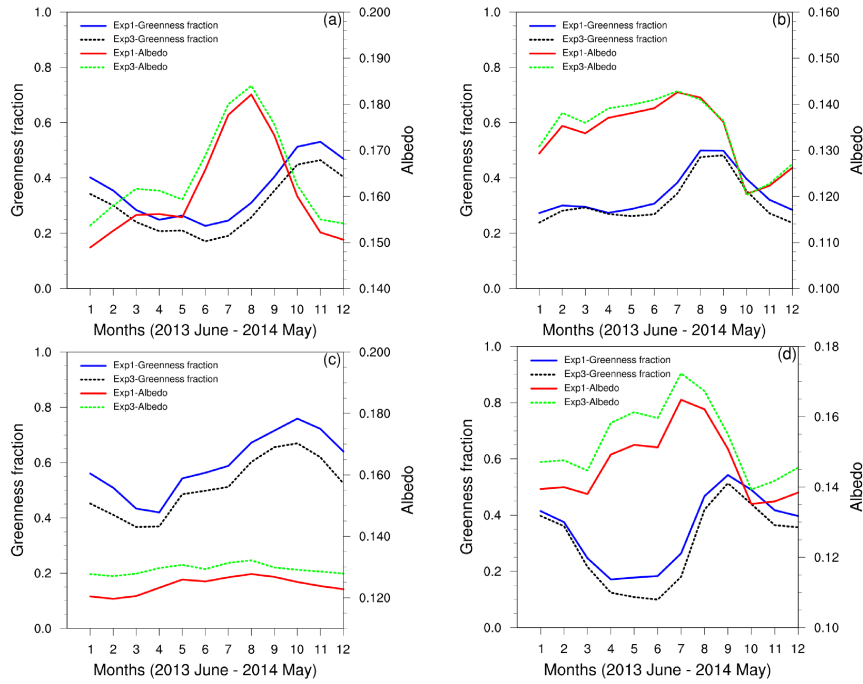


**Fig. 10** Time series of monthly mean albedo and greenness fraction spatially averaged over Western ghats (a), North India (b), Northeast India (c), and Central India (d) for Exp1 run and Exp3 run, respectively.

**Table 3** The annual mean change of Latent heat flux, Sensible heat flux, Soil moisture, Soil temperature, and Net surface radiation due to historic land cover change (1930-2013) from forest (Evergreen needle leaf (ENL), Evergreen broadleaf (EBL), Deciduous broadleaf (DBL), Mixed forest (MF) ) to cropland, grassland, urbanland, and open shrub land respectively over Western ghats, North India, Northeast India and Central India. Student's *t*-test are performed and entries with 90% and 95% statistical significance level are indicated by (underlined) and (\*), respectively.

Region	Landcover change	LHF( $W/m^2$ )	SHF( $W/m^2$ )	SM( $m^3/m^3$ )	ST(K)	NSR( $W/m^2$ )
Western Ghats	EBL to Crop	-26.55*	-14.79*	-0.06*	0.71	-11.87*
	EBL to Grass	-31.85*	<u>19.65</u>	-0.04	1.12	-11.23*
	EBL to Open shrub	-43.74*	24.06*	-0.02	<u>1.85</u>	-22.07*
North India	ENL to Crop	-16.29*	-1.62	0.05*	0.58	-7.72
	ENL to Open shrub	-23.06*	-0.54	0.07*	1.37	-13.05
	MF to Open shrub	-19.60*	14.51*	0.08*	1.46	-8.98
Northeast India	EBL to Crop	-25.57*	10.50	-0.07	0.85	-6.31
	EBL to Grass	-27.93*	17.55*	-0.05	1.12	-8.30
	EBL to Open shrub	35.83*	21.09*	-0.04	2.00	-22.53*
	ENL to Open shrub	-33.56*	15.10*	0.01	1.57	-23.55*
Central India	MF to Crop	-15.60	2.91	-0.02	0.76	-14.79

### 362 4.3 Impact on land surface characteristics due to the change of different landcover classes over the 363 Indian domain

364 Table 3 shows the impact of dominant land cover change (1930-2013) on land surface characteristics  
365 such as LHF, SHF, SM, ST and NSR over Western Ghats, North India, Northeast India, and Central  
366 India. The annual change of LHF, SHF, SM, ST and NSR depicted in Table 3 is only averaged over  
367 the grid points in a particular region where the above mentioned landcover change has been observed

**Table 4** The annual mean change of Latent heat flux, Sensible heat flux, Soil moisture, Soil temperature, and Net surface radiation due to historic land cover change (1930-2013) from forest (Evergreen needle leaf (ENL), Evergreen broadleaf (EBL), Deciduous broadleaf (DBL), Mixed forest (MF) ) to cropland, grassland, urbanland, and open shrub land respectively. Student's *t*-test are performed and entries with 90% and 95% statistical significance level are indicated by (underlined) and (\*), respectively.

Variable	Forest type	Crop	Grass	Urban	Open shrub
Latent heat flux ( $W/m^2$ )	ENL	-16*	-19*	-66.83*	-25*
	EBL	-25.63*	-29.81*	-74.08*	-40.11*
	DBL	-17.43*	-21.38*	-57.19*	-31.05*
	MF	-13.52*	-15.08*	-62.44*	-23.29*
Sensible heat flux ( $W/m^2$ )	ENL	<u>-11.71</u>	9.46*	49.59*	13.92*
	EBL	-13.46*	16.69*	67.05*	21.21*
	DBL	<u>-14.09</u>	8.41*	44.51*	<u>2.11</u>
	MF	-17.11*	-17.13*	45.94*	-15.88*
Soil moisture ( $m^3/m^3$ )	ENL	0.06*	0.06*	0.13*	0.07*
	EBL	-0.06*	-0.05*	0.08*	-0.02
	DBL	-0.07*	<u>-0.08</u>	0.11*	-0.01
	MF	0.05*	0.06*	0.14*	0.07*
Soil temperature (K)	ENL	0.45	0.55	3.17	1.44
	EBL	0.76	1.07	2.85*	<u>1.91</u>
	DBL	0.36	0.65	2.67	1.51
	MF	0.53	0.59	2.93	<u>1.42</u>
Net surface radiation ( $W/m^2$ )	ENL	-9.83*	-10.74*	-20.77*	-18.90*
	EBL	-11.52*	-11.02*	-13.81*	-21.49*
	DBL	-11*	-9.88*	-19.08*	-18.68*
	MF	-11.69*	-11.75*	-16.73*	-15.56*

368 from the year 1930 to 2013, respectively. A two-tailed student's *t*-test is performed for corroborating  
369 the statistical significance of the results of Table 3. Entries in the Table 3 with "\*" indicates 95% of  
370 statistical significance level, while the underlined entries indicate 90% of statistical significance level.  
371 From Table 3 it is clear that all landcover changes from forest (ENL, EBL, DBL and MF) to other  
372 landcover types such as cropland, grassland, urban and open shrubland, show a consistent reduction in  
373 latent heat flux values. Table 3 shows that the reduction is maximum for the land cover change from  
374 forest to open shrubland, followed by landcover change from forest to grassland and finally from forest  
375 to cropland. The above mentioned observation can be explained since the greenness fraction is lower in  
376 open shrubland as compared to cropland, and grassland, respectively. Furthermore, evapotranspiration  
377 values are lower for the open shrubland as compared to grassland and cropland, respectively. Over the  
378 Western ghats and Northeast India, the reduction in LHF is large for the landcover change from EBL  
379 forest to grassland as compared to landcover change from EBL forest to cropland. The reason for the  
380 above is that the deeper extended root depth and higher greenness fraction of cropland results in higher  
381 evapotranspiration for the cropland as compared to grassland. The above results are consistent with the  
382 earlier studies Duveiller et al. (2018). The statistically significant results show an increase in sensible heat  
383 flux when the forest land cover changes to other land cover types except for the cropland, which shows  
384 a decrease in sensible heat flux. Like the latent heat flux, the maximum change in sensible heat flux is

also for the change from forest land cover to open shrubland followed by change from forest to grassland and cropland, respectively. The above observation is easily explained since any decrease in latent heat flux leads to a corresponding increase in the sensible heat flux, by invoking the surface energy balance. Except for North India, all the other three regions show a decrease in soil moisture estimates when the land cover changes from forest to other land cover types. Over the Western Ghats, the largest change in soil moisture values for the land cover change from EBL to cropland has a value of  $-0.06 \text{ m}^3/\text{m}^3$  which is statistically significant at the 95% level. Over North India, the land cover changes from ENL to cropland, ENL to open shrubland, and MF to open shrubland show an increase in the soil moisture values. The above results for North India are at variance with the expected trend and is due to the nature of the soil texture of the corresponding land cover type observed over North India. All three land cover changes over North India from forest to other land cover types result in soil texture with higher porosity which contributes to increase in soil moisture. All land cover changes from forest to cropland, from forest to grassland, and from forest to open shrubland show an increase in soil temperature values. However, the changes in soil temperature are significant only for (up to 90% significant level) the land cover change from EBL forest to open shrubland over the Western ghats with a value of 1.85 K. The above feature is consistent with the fact that the maximum negative change in latent heat flux and maximum positive change in sensible heat flux also correspond to the land cover change from EBL to open shrubland. The NSR flux values show a consistent reduction for all land cover changes from forest to other land cover types. This is attributed to the higher albedo values of open shrubland as compared to the albedo values of grassland and cropland, respectively.

Annual mean change of surface fluxes (LHF and SHF), SM, and soil temperature (ST) for the land cover changes from forest to crops, grassland, open shrubland, and urban land over the Indian domain due to historical land cover changes (1930-2013) are shown in Table 4. Table 4 is similar to Table 3 in the sense that the mean change of LHF, SHF, SM, ST and NSR are only averaged over the grid points over India when the above mentioned landcover changes has been observed from the year 1930 to 2013, respectively. Results from Table 4 indicate a consistent decrease in LHF values in all four cases. Since the cropland (CL), grassland (GL), open shrubland (OSL), and urban land (UL) have lower evapotranspiration values as compared to forest, the above is consistent with a decrease of LHF from forest to other landcover types (Kvalevåg et al., 2010). The annual mean change in LHF is highest for landcover change to UL compared to other land cover classes and is attributed to the low greenness fraction values and the limited impervious fraction of water over the UL. The evergreen broadleaf forest (EBF) has the largest change in the annual mean LHF as compared to other forest types. With EBL, the change in LHF is maximum for UL ( $-74.08 \text{ W}/\text{m}^2$ ) followed by OSL ( $-40.11 \text{ W}/\text{m}^2$ ), GL ( $-29.81 \text{ W}/\text{m}^2$ ) and CL ( $-25.63 \text{ W}/\text{m}^2$ ). The above is attributed to the high greenness fraction values and higher root depth of EBL forest compared to other forest types. Additionally, the evapotranspiration is higher for CL than GL due to the high greenness fraction and high root depth of CL as compared to GL. Table 4 reveals that the mean annual change in SHF is higher for all the land cover changes from forest to other landcover types except for the land cover change from forest to CL. This may be attributed to the albedo effect playing a significant role as compared to evapotranspiration for the landcover change from forest to cropland. The increase in SHF for the land cover change from EBF to GL is consistent with the results of Duveiller et al. (2018). Similar to LHF, the annual mean change in SHF is highest

426 for the land cover change from forest to UL compared to other landcover types and is due to the high  
427 albedo associated with UL as compared to the albedo values of GL and CL, respectively. Table 4 shows a  
428 consistent reduction in NSR values for all land cover changes from forest to CL, OSL, GL, and UL. Land  
429 cover change from forest to short vegetation over the tropics is generally associated with an increase  
430 in surface albedo, contributing to the decrease of NSR. The landcover change to OSL shows a large  
431 annual decrease in NSR values as compared to GL and CL types, respectively since the albedo values  
432 are higher for OSL as compared to the albedo value of GL and CL, respectively. The historical land cover  
433 change from forest to CL, GL, OSL, and UL contribute to increasing the soil temperature (ST). The  
434 deforestation studies of Kvalevåg et al. (2010) and Halder et al. (2016) over Indian domain also show an  
435 increase in surface temperature. The highest annual mean change of 2.85 K in ST is associated with the  
436 landcover change from EBL forest to UL, the above meeting the 95% statistical significance level. The  
437 above feature is attributed to the high greenness fraction of the EBL forest. Furthermore, the evaporative  
438 cooling is low over UL as compared to OSL, GL, and CL, respectively. Results of regional studies over  
439 the Indian domain also indicate that the urbanization scenario has contributed to an increase in the  
440 surface temperature (Li et al., 2017). The annual mean change in ST is significant for UL, followed by  
441 OSL, GL, and CL. This is because the canopy coverage can shade the soil surface, which lowers ST;  
442 the canopy coverage is more for the CL followed by GL and OSL. Conversion of EBL forest to open  
443 shrubland shows an increase in ST by 2.11 K with 90% of the statistical significance level. The land  
444 cover change for the forest type ENL and MF show an increase in soil moisture, when the land cover is  
445 changed to non-forest type. However, the EBL and DBL forest types show a decrease in soil moisture  
446 when the land cover is changed to non-forest type with the above meeting the 95% statistical significance  
447 level. Results indicate that the annual mean of latent heat flux and net surface radiation reduced by  
448  $-24.74 W/m^2$  and  $-14.18 W/m^2$  while the soil temperature and sensible heat flux increased by 2.78 K  
449 and  $4.97 W/m^2$ , respectively. Due to reasons of brevity, the results of Ctl-run are not shown.

## 450 5 Conclusion

451 The present study utilized the Noah LSM to study the impacts of historical land cover changes on land  
452 surface characteristics from 1930-2013. Four simulations are performed using Noah LSM, (i) Ctl-run,  
453 and (ii) to (iv) the three Experiment runs. Ctl-run is simulated using MODIS-IGBP land cover, NCEP  
454 albedo, and NCEP greenness fraction data, while the three experimental runs are simulated using three  
455 different potential land cover maps (1930, 1975, and 2013), and associated with modified albedo, and  
456 modified greenness fraction data. For the analysis, four regions are selected, where the land cover changes  
457 are clearly discernable, namely, Western ghats, North India, Central India, and Northeast India.

458 Results indicate that land cover change (1930 to 2013) reduces latent heat flux and net surface  
459 radiation in all the four regions and for all the seasons. The above behavior can be explained by invoking  
460 the decrease of evapotranspiration and the increase of albedo in all the four regions for the Exp-3 run.  
461 The land cover change from forest to other land cover types resulted in increased sensible heat flux and  
462 soil temperature for all four regions and for all the seasons. This is attributed to the fact that reduced  
463 latent heat flux results in Exp-3 run contributing to an increase in the sensible heat flux by invoking  
464 the surface energy balance. Also, the reduced greenness fraction due to land cover change from forest to

other land cover types can increase the amount of radiation that reaches the land surface, resulting in the surface warming effect. The land cover change from forest to other land cover types decreases the soil moisture for all regions except for North India, where the soil moisture estimate increases and shows a different behavior. Results show that the maximum annual mean change in latent heat flux and net surface radiation is for the land cover change from the forest (EBL, ENL, MF) to open shrubland as compared to forest to grassland and forest to cropland, due to low evapotranspiration and high albedo for open shrubland type as compared to grassland and cropland types. The soil temperature increases for all land cover changes from forest to other land cover types for all regions; however, the land cover change from EBL to open shrubland over Western ghats shows the highest increase in soil temperature having a value of 1.85 K, the above meeting the 90% statistical significance level. Over North India, the soil moisture estimates increases due to land cover change from forest to other land cover types, which is attributed to the soil texture of the corresponding land cover class over North India. The results are consistent with regional results. Over the Indian domain, the maximum change in latent heat flux and sensible heat flux correspond to the land cover change from forest to urban land as compared to the forest to cropland, forest to open shrubland, and forest to grassland. Land cover change from EBL to urban land shows the maximum decrease in latent heat flux ( $-74.08 W/m^2$ ) and maximum increase in sensible heat flux ( $67.05 W/m^2$ ), both meeting the 95% of the statistical significance level. Results indicate that the annual mean of latent heat flux and net surface radiation is reduced by  $-24.74 W/m^2$  and  $-14.18 W/m^2$ , while the sensible heat flux and soil temperature increases by  $4.97 W/m^2$  and 2.78 K.

## ACKNOWLEDGEMENTS

The authors thank the Hydrological Sciences Laboratory at NASA's Goddard Space Flight Center (GSFC) for providing the LIS (Land Information System). The Research Application Laboratory (RAL), National Center for Atmospheric Research (NCAR), USA is acknowledged for providing the 1D Noah LSM. The authors acknowledge the National Remote Sensing Centre, Indian Space Research Organization (ISRO) for providing the fractional forest cover data. The first author (Vibin Jose) also thanks the Council of Science and Industrial Research (CSIR), Government of India for providing Research Fellowship. The authors also gratefully acknowledge the Director of IIST (Indian Institute of Space Science and Technology) for the support, encouragement and for providing the High-Performance Computing (HPC) facility.

## Conflicts of Interest

The authors declare no conflict of interest.

## Funding

The present study has not received any specific grant or funding from any agency.

---

**499 Availability of data and material**

500 The data sets and material used in the present study are freely available in the web.

**501 Code availability**

502 The codes employed in this study are available to be shared on request.

**503 Ethics approval**

504 The authors declare that the contents and the results of the manuscript have not been published in any  
505 other journal or conference.

**506 Consent to participate and Consent for publication**

507 The authors provide their consent and willingness to participate in the publication process and to publish  
508 the above manuscript.

**509 Disclosure statement**

510 No conflict of interest is reported by the authors.

**511 References**

- 512 Anyanwu C (2015) The impact of deforestation on soil conditions in anambra state of nigeria. *Agriculture,*  
513 *Forestry and Fisheries* 4:64, DOI 10.11648/j.aff.s.2015040301.21
- 514 Betts R (2001) Biogeophysical impacts of land use on present-day climate: Near-surface temperature  
515 and radiative forcing. *Atmospheric Science Letters* 2:39 – 51, DOI 10.1006/asle.2001.0037
- 516 Betts R, Falloon P, Klein Goldewijk K, Ramankutty N (2007) Biogeophysical effects of land use on  
517 climate: Model simulations of radiative forcing and large-scale temperature change. *Agricultural and*  
518 *Forest Meteorology* 142:216–233, DOI 10.1016/j.agrformet.2006.08.021
- 519 Bonan G (2008) *Forests and climate change: Forcings, feedbacks, and the climate benefits of forests.*  
520 *Science (New York, NY)* 320:1444–1449, DOI 10.1126/science.1155121
- 521 Bounoua L, Defries R, Collatz G, Sellers P, Khan H (2002) Effects of land cover conversion on surface  
522 climate. *cc* 52:29–, DOI 10.1023/A:1013051420309
- 523 Bright R, Davin E, O’Halloran T, Pongratz J, Cescatti A (2017) Local temperature response to land  
524 cover and management change driven by non-radiative processes. *Nature Climate Change* 7:296–302,  
525 DOI 10.1038/nclimate3250
- 526 Chase T (1999) The role of historical land-cover changes as a mechanism for global and regional climate  
527 change. PhD thesis, Colorado State University

- 528 Chen F, Mitchell K, Schaake J, Xue Y, Pan HL, Koren V, Duan QY, Ek M, Betts A (1996) Modeling of  
529 land surface evaporation by four schemes and comparison with field observations. *Journal of Geophysical*  
530 *Research: Atmospheres* 101(D3):7251–7268
- 531 Cherubini F, Huang B, Hu X, Tölle M, Strømman A (2018) Quantifying the climate response to extreme  
532 land cover changes in Europe with a regional model. *Environmental Research Letters* 13, DOI 10.1088/  
533 1748-9326/aac794
- 534 Davin E, de NOBLET N (2010) Climatic impact of global-scale deforestation: Radiative versus nonra-  
535 diative processes. *Journal of Climate - J CLIMATE* 23, DOI 10.1175/2009JCLI3102.1
- 536 Deng X, Zhao C, Yan H (2013) Systematic modeling of impacts of land use and land cover changes on  
537 regional climate: A review. *Advances in Meteorology* 2013, DOI 10.1155/2013/317678
- 538 Dirmeyer AP, Niyogi D, Noblet-Ducoudre ND, Dickinson RE, Snyder PK (2010) Impacts of land use  
539 change on climate. *International Journal of Climatology* 30:1905–1907
- 540 Dirmeyer PA, Halder S (2016) Sensitivity of numerical weather forecasts to initial soil moisture variations  
541 in cfsv2. *Weather and Forecasting* 31(6):1973–1983
- 542 Dong N, Liu Z, Luo M, Fang C, Lin H (2019) The effects of anthropogenic land use changes on climate  
543 in China driven by global socioeconomic and emission scenarios. *Earth's Future* 7(7):784–804, DOI  
544 <https://doi.org/10.1029/2018EF000932>
- 545 Dutta S, Das S, Kar S, Mohanty UC, Joshi P (2009) Impact of vegetation on the simulation of seasonal  
546 monsoon rainfall over the Indian subcontinent using a regional model. *Journal of Earth System Science*  
547 118, DOI 10.1007/s12040-009-0048-z
- 548 Duveiller G, Hooker J, Cescatti A (2018) The mark of vegetation change on Earth's surface energy  
549 balance. *Nature Communications* 9, DOI 10.1038/s41467-017-02810-8
- 550 Feddema J, Oleson K, Bonan G, Mearns L, Washington W, Meehl G, Nychka D (2005) A com-  
551 parison of a GCM response to historical anthropogenic land cover change and model sensitivity  
552 to uncertainty in present-day land cover representations. *Climate Dynamics* 25:581–609, DOI  
553 10.1007/s00382-005-0038-z
- 554 Findell KL, Knutson TR, Milly PCD (2006) Weak simulated extratropical responses to complete trop-  
555 ical deforestation. *Journal of Climate* 19(12):2835 – 2850, DOI 10.1175/JCLI3737.1, URL <https://journals.ametsoc.org/view/journals/clim/19/12/jcli3737.1.xml>
- 557 Friedl M, McIVER D, Hodges J, Zhang X, Muchoney D, Strahler A, Woodcock C, Gopal S, Schneider  
558 A, Cooper A, Baccini A, Gao F, Schaaf C (2002) Global land cover mapping from MODIS: Algorithms  
559 and early results. *Remote Sensing of Environment* 83:287, DOI 10.1016/S0034-4257(02)00078-0
- 560 Garratt J (1993) Sensitivity of climate simulations to land-surface and atmospheric boundary-layer  
561 treatments—a review. *Journal of Climate; (United States)* 6:3, DOI 10.1175/1520-0442(1993)006<0419:  
562 SOCSTL>2.0.CO;2
- 563 Gogoi P, VINOJ V, Swain D, Roberts G, Dash J, Tripathy S (2019) Land use and land cover change effect  
564 on surface temperature over eastern India. *Scientific Reports* 9, DOI 10.1038/s41598-019-45213-z
- 565 Gruber A, Dorigo W, Crow W, Wagner W (2017) Triple collocation-based merging of satellite soil  
566 moisture retrievals. *IEEE Transactions on Geoscience and Remote Sensing* PP:1–13, DOI 10.1109/  
567 TGRS.2017.2734070

- 568 Guo W, Wang X, Sun J, Ding A, Jun Z (2016) Comparison of land-atmosphere interaction at different  
569 surface types in the mid- to lower reaches of the yangtze river valley. *Atmospheric Chemistry and*  
570 *Physics* 16:9875–9890, DOI 10.5194/acp-16-9875-2016
- 571 Halder S, Saha S, Dirmeyer P, Chase T, Goswami BN (2016) Investigating the impact of land-use  
572 land-cover change on indian summer monsoon daily rainfall and temperature during 1951–2005 us-  
573 ing a regional climate model. *Hydrology and Earth System Sciences* 20:1765–1784, DOI 10.5194/  
574 hess-20-1765-2016
- 575 Hansen J, Sato M, Ruedy R, Nazarenko L, Lacis A, Schmidt G, Russell G, Aleinov I, Bauer M, Bauer  
576 S, Bell N, Cairns B, Canuto V, Chandler M, Cheng Y, Delgenio A, Faluvegi G, Fleming E, Friend  
577 A, Zhang S (2005) Efficacy of climate forcings. *Journal of Geophysical Research* 110, DOI 10.1029/  
578 2005JD005776
- 579 Huang H, Xue Y, Chilukoti N, Liu Y, Chen G, Diallo I (2020) Assessing global and regional ef-  
580 fects of reconstructed land-use and land-cover change on climate since 1950 using a coupled  
581 land-atmosphere-ocean model. *Journal of Climate* DOI 10.1175/JCLI-D-20-0108.1
- 582 Kolassa J, Gentine P, Prigent C, Aires F, Alemohammad S (2017) Soil moisture retrieval from AMSR-E  
583 and ASCAT microwave observation synergy. part 2: Product evaluation. *Remote Sensing of Environ-*  
584 *ment* 195:202–217, DOI 10.1016/j.rse.2017.04.020
- 585 Kumar S, Peters-Lidard C, Tian Y, Houser P, Geiger J, Olden S, Lighty L, Eastman J, Doty B, Dirmeyer  
586 P, Adams J, Mitchell K, Wood E, Sheffield J (2006) Land information system: An interoperable  
587 framework for high resolution land surface modeling. *Environmental Modelling & Software* 21(10):1402  
588 – 1415, DOI <https://doi.org/10.1016/j.envsoft.2005.07.004>
- 589 Kvalevåg M, Myhre G, Bonan G, Levis S (2010) Anthropogenic land cover changes in a gcm with  
590 surface albedo changes based on modis data. *International Journal of Climatology* 30:2105 – 2117,  
591 DOI 10.1002/joc.2012
- 592 Lawrence P, Chase T (2010) Investigating the climate impacts of global land cover change in the commu-  
593 nity climate system model. *International Journal of Climatology* 30:2066 – 2087, DOI 10.1002/joc.2061
- 594 Lee SJ, Berbery E (2012) Land cover change effects on the climate of the la plata basin. *Journal of*  
595 *Hydrometeorology* 13:84–102, DOI 10.1175/JHM-D-11-021.1
- 596 Li X, Mitra C, Dong L, Yang Q (2017) Understanding land use change impacts on microclimate using  
597 weather research and forecasting (wrf) model. *Physics and Chemistry of the Earth, Parts A/B/C* 103,  
598 DOI 10.1016/j.pce.2017.01.017
- 599 Liu F, Tao F, Liu J, Zhang S, Xiao D, Wang M, Zhang H, Huizi B (2014) Effects of land use/cover  
600 change on land surface energy partitioning and climate in northeast china. *Theoretical and Applied*  
601 *Climatology* 123, DOI 10.1007/s00704-014-1340-7
- 602 Liu Y, Guo W, Song Y (2015) Estimation of key surface parameters in semi-arid region and their  
603 impacts on improvement of surface fluxes simulation. *Science China Earth Sciences* 59, DOI 10.1007/  
604 s11430-015-5140-4
- 605 Liu Y, Xue Y, MacDonald G, Cox P, Zhang Z (2019) Global vegetation variability and its response to  
606 elevated  $\text{CO}_2$ , global warming, and climate variability – a study using the offline *ssib4/trifid*  
607 model and satellite data. *Earth System Dynamics* 10:9–29, DOI 10.5194/esd-10-9-2019

- 608 Lozano-Parra J, Pulido M, Lozano C, Schnabel S (2018) How do soil moisture and vegetation covers influ-  
609 ence soil temperature in drylands of mediterranean regions? *Water* 10:1747, DOI 10.3390/w10121747
- 610 McColl KA, Vogelzang J, Konings AG, Entekhabi D, Piles M, Stoffelen A (2014) Extended triple collo-  
611 cation: Estimating errors and correlation coefficients with respect to an unknown target. *Geophysical*  
612 *Research Letters* 41(17):6229–6236, DOI 10.1002/2014GL061322
- 613 Nair A, Indu J (2019) Improvement of land surface model simulations over india via data assimilation  
614 of satellite-based soil moisture products. *Journal of Hydrology* 573:406–421, DOI 10.1016/j.jhydrol.  
615 2019.03.088
- 616 Nair U, Wu Y, Kala J, Lyons T, Pielke Sr R, Hacker J (2011) The role of land use change on the  
617 development and evolution of the west coast trough, convective clouds, and precipitation in southwest  
618 australia. *Journal of Geophysical Research* 116, DOI 10.1029/2010JD014950
- 619 Niu C, Musa A, Liu Y (2015) Analysis of soil moisture condition under different land uses in the arid  
620 region of horqin sandy land, northern china. *Solid Earth* 6, DOI 10.5194/se-6-1157-2015
- 621 Niyogi D, Kishtawal C, Tripathi S, Govindaraju R (2010) Observational evidence that agricultural  
622 intensification and land use change may be reducing the indian summer monsoon rainfall. *Water*  
623 *Resources Research - WATER RESOUR RES* 46, DOI 10.1029/2008WR007082
- 624 Niyogi D, Mohanty UC, Kishtawal C, Ghosh S, Nair U, Ek M, Rajeevan M (2018) The Impact of  
625 Land Cover and Land Use Change on the Indian Monsoon Region Hydroclimate, pp 553–575. DOI  
626 10.1007/978-3-319-67474-2\_25
- 627 Pai D, Sridhar L, Rajeevan M, Sreejith OP, Satbhai N, Mukhopadhyay B (2014) Development of a new  
628 high spatial resolution ( $0.25^\circ \times 0.25^\circ$ ) long period (1901–2010) daily gridded rainfall data set over  
629 india and its comparison with existing data sets over the region. *Mausam* 65:1–18
- 630 Peng S, Piao S, Zeng Z, Ciais P, Zhou L, Li L, Myneni R, Yin Y, Zeng H (2014) Afforestation in china  
631 cools local land surface temperature. *Proceedings of the National Academy of Sciences of the United*  
632 *States of America* 111, DOI 10.1073/pnas.1315126111
- 633 Pielke RA, Avissar R, Raupach M, Dolman AJ, Zeng X, Denning AS (1998) Interactions between the  
634 atmosphere and terrestrial ecosystems: influence on weather and climate. *Global Change Biology*  
635 4(5):461–475, DOI <https://doi.org/10.1046/j.1365-2486.1998.t01-1-00176.x>
- 636 Pielke RA, Pitman A, Niyogi D, Mahmood R, Mcalpine C, Hossain F, Klein Goldewijk K, Nair U, Betts  
637 R, Fall S, Reichstein M, Kabat P, de NOBLET N (2011) Land use/land cover changes and climate:  
638 Modeling analysis and observational evidence. *Wiley Interdisciplinary Reviews: Climate Change* 2:828  
639 – 850, DOI 10.1002/wcc.144
- 640 Pitman A, de NOBLET N, Avila F, Alexander L, Boisier JP, Brovkin V, Delire C, Cruz F, Donat  
641 M, Gayler V, Hurk B, Reick C, Voltaire A (2012) Effects of land cover change on temperature and  
642 rainfall extremes in multi-model ensemble simulations. *Earth System Dynamics* 3:213–231, DOI 10.  
643 5194/esd-3-213-2012
- 644 Pitman AJ (2003) The evolution of, and revolution in, land surface schemes designed for climate models.  
645 *International Journal of Climatology* 23(5):479–510, DOI <https://doi.org/10.1002/joc.893>
- 646 Reddy CS, Saranya K, Shaik V, Satish K, Jha C, Diwakar P, Dadhwal V, Rao P, Murthy Y (2018)  
647 Assessment and monitoring of deforestation and forest fragmentation in south asia since the 1930s.  
648 *Global and Planetary Change* 161:132–148, DOI 10.1016/j.gloplacha.2017.10.007

- 649 Rodell M, Houser PR, Jambor U, Gottschalck J, Mitchell K, Meng CJ, Arsenault K, Cosgrove B,  
650 Radakovich J, Bosilovich M, Entin JK, Walker JP, Lohmann D, Toll D (2004) The global land data  
651 assimilation system. *Bulletin of the American Meteorological Society* 85(3):381–394, DOI 10.1175/  
652 BAMS-85-3-381
- 653 Rodell M, Houser PR, Berg AA, Famiglietti JS (2005) Evaluation of 10 methods for initializing a land  
654 surface model. *Journal of Hydrometeorology* 6(2):146–155, DOI 10.1175/JHM414.1
- 655 Sampaio G, Nobre C, Costa M, Satyamurty P, Filho B, Cardoso M (2007) Regional climate change over  
656 eastern amazonia caused by pasture and soybean cropland expansion. *Geophysical Research Letters -*  
657 *GEOPHYS RES LETT* 34, DOI 10.1029/2007GL030612
- 658 Stoffelen A (1998) Toward the true near-surface wind speed: Error modeling and calibration using triple  
659 collocation. *Journal of Geophysical Research: Oceans* 103(C4):7755–7766, DOI 10.1029/97JC03180
- 660 Tyagi J, Qazi N, Rai SP, Singh M (2013) Analysis of soil moisture variation by forest cover structure in  
661 lower western himalayas, india. *Journal of Forestry Research* 24, DOI 10.1007/s11676-013-0355-8
- 662 Wu X, Lu G, Wu Z, He H, Scanlon T, Dorigo W (2020) Triple collocation-based assessment of satellite  
663 soil moisture products with in situ measurements in china: Understanding the error sources. *Remote*  
664 *Sensing* 12(14), DOI 10.3390/rs12142275